Russian Journal of Earth Sciences

Special Issue: "25th anniversary of the Russian Journal of Earth Sciences"

A Global View on Internal Tides

E. G. Morozov[1,2]

[1]Shirshov Institute of Oceanology, Russian Academy of Sciences, Moscow, Russia
[2]Moscow Institute of Physics and Technology, Moscow, Russia
* **Correspondence to:** E. G. Morozov, egmorozov@mail.ru

Abstract: This is a review paper on generation of internal tides in the global ocean based on literature data and publications of the author. Energy fluxes of semidiurnal internal tide generation over submarine ridges were estimated based on modeling and measurements on moorings in many regions of the ocean. Data from 4000 moorings during a period of 50 years are considered. Regions of intense generation of internal tides are indicated. They are related to several underwater oceanic ridges. Energy fluxes from submarine ridges greatly exceed those from the continental slopes because generally the currents of the barotropic tide are parallel to the coastline. If the barotropic tide currents are normal to the ridge, they generate strong internal tides. They account approximately for one fourth of the energy losses of the barotropic tide. Decay of internal tide during propagation was estimated based on the data from lines of moorings located normal to the ridges. Model simulations and moored measurements result in a global map of semidiurnal internal tide amplitudes.

Keywords: Internal tides, bottom topography, overflows, submarine ridges, tidal energy dissipation.

Citation: Morozov E. G. (2024), A Global View on Internal Tides, *Russian Journal of Earth Sciences*, Vol. 24, ES1009, https://doi.org/10.2205/2024ES000898

1. Introduction

American scientist and politician Benjamin Franklin was the first to notice the existence of internal waves. In 1762, he described the waves at the interface between oil and water in a ship's lantern. More than 100 years passed since F. Nansen made observations of internal waves in the sea [*Nansen*, 1902] using water sampling bottles. Intense studies of internal waves began only in the 1960s [*LaFond*, 1961; *Lee and Cox*, 1966; *Summers and Emery*, 1963]. In this decade measurements on moorings revealed the existence of strong oscillations at tidal periods [*Cairns and LaFond*, 1966].

However, our knowledge of internal waves by the 1960s was quite poor, especially about the existence of internal tides. This was very briefly written in the book by W. Krauss [*Krauss*, 1966]. A paper by W. Munk [*Munk*, 1966] was published on the influence of tides on the entire dynamics of the ocean and especially on internal tides, but it was not yet deeply understood at that time. It is likely that the paper by Tareev [*Tareev*, 1966] was the only publication on internal waves in Russia, but it has not been associated yet with internal tides. The Garrett-Munk model describing the background state of the internal wave field appeared only in 1972 [*Garrett and Munk*, 1972]. The authors presented a model of dimensionless energy of internal waves, from which the observed spectra of temperature fluctuations and currents on moored buoys and the spectra measured by towed instruments were obtained. A brilliant American experiment in the technical sense to study internal waves (IWEX) was conducted in 1973 [*Briscoe*, 1975]. A pyramidal construction with one mutual buoyancy moored at three spatially separated locations was set in the Sargasso Sea where internal waves are very weak. However, at that time, the scientists did not know that internal tides in the Sargasso Sea are weak. In 1975, C. Wunsch published two review works summarizing the current knowledge about internal tides [*Wunsch*, 1975a,b].

Research Article

Received: 15 October 2023
Accepted: 15 January 2024
Published: 29 February 2024

The propagation of internal disturbances along inclined characteristic surfaces (which fall into the category of attractors, that is, the concentration of disturbances occurs around specific trajectories) was first described by Phillips [*Phillips*, 1977]. The finding of Phillips [*Phillips*, 1977] that unlike surface waves the motion of water particles in internal waves occurs along sloping lines was continued with the idea that generation of internal tides over sloping bottom occurs because when currents of the barotropic tide overflow topography the most intense generation of internal tides occurs over submarine slopes if their inclination is close to the inclination of internal wave characteristic curves $\frac{dz}{dx} = \frac{k_z}{k_x} = \sqrt{\frac{\omega^2 - f^2}{N^2 - \omega^2}}$ [*Baines*, 1982; *Holloway and Merrifield*, 2003; *Johnston et al.*, 2003; *Phillips*, 1977; *Torgrimson and Hickey*, 1979] (Figure 1). Usually this happens in the upper parts of the submarine ridges and in the regions of the shelf break where stratification is strong [*Hibiya*, 2004].

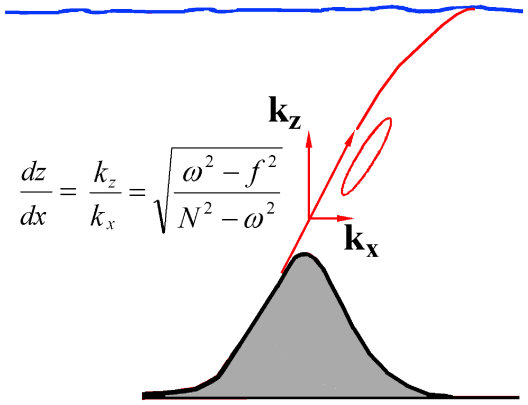

Figure 1. Scheme of internal wave beam. Excursion of water particles is shown by an elongated ellipse. Beam of internal perturbations is shown in red. Underwater topography is in gray. Formula describes the slope of internal wave beam.

Joint efforts of many scientists resulted in the idea that internal tides are generated by the barotropic tide currents flowing over sloping topography; thus, the vertical component of tidal currents periodically displaces isopycnals [*Baines*, 1982; *Morozov*, 1995, 2018; *Sjöberg and Stigebrandt*, 1992]. The frequency of these displacements is tidal. Internal waves are generated by periodical displacements of isopycnals and propagate from the sloping topography: continental slopes, submarine ridges, and seamounts. Numerous investigations show that tidal interactions and wind are the main sources of internal wave generation [*Garrett and Kunze*, 2007; *Munk*, 1966; *Munk and Wunsch*, 1998].

2. Energy fluxes of internal tides from bottom topography

Baines [*Baines*, 1982] used the following approach when studying generation of internal tides over continental slopes. After solving the equation system, he found an expression for mass force F that is responsible for internal wave generation; this force is nonzero over sloping topography:

$$\overrightarrow{F} = \frac{QN^2}{\omega} z \overrightarrow{\overrightarrow{z}} \frac{\partial h}{\partial x} \frac{1}{h^2} \sin \omega t.$$

Here, Q is the water transport by the barotropic tide; $z = h(x)$ is the ocean bottom; ω is the tidal frequency; N is the Brunt-Väisälä frequency. This mass force is non-zero only in regions with variable depth due to the presence of the derivative of depth with respect to the horizontal coordinate in this formula: $h'(x)$.

Submarine ridges are important regions of internal tide generation [*Morozov*, 1995; *Sjöberg and Stigebrandt*, 1992]. The generation of internal tides over the slopes of ridges exceeds many times the generation over continental slopes. This result was reported by Morozov [*Morozov*, 1995]. After the first publication, the results and estimates were

updated. This paper is a progressive report on internal tides in the global ocean and geographical distribution of semidiurnal internal tide, its amplitudes, and energy. The goal of this research is to apply observations and modeling to understand the distribution of internal tide energy and amplitudes over the global ocean.

As was previously written, P. Baines solved the equations, calculated the mass forces and energy of the internal tide over most of the continental slopes. Morozov [*Morozov*, 1988, 1995] continued this work and calculated the energy of the internal tide over most of the underwater ridges (more than 50 ridges). These modeling estimates were compared to the field observations on moorings. The results were repeatedly updated and published [*Morozov*, 1988, 1990, 1995, 2006, 2018]. This publication is an updated review of previous publications.

The estimated energies from all major ridges and island arcs in each ocean have been summed. Calculations from previous publications were updated to get more correct estimates of energy fluxes. The resulting sums of the energy of semidiurnal internal waves per time unit (power) in the three oceans (including the Southern Ocean as the southern parts of the three) are the following:

- 3.1×10^{11} W in the Atlantic;
- 2.8×10^{11} W in the Pacific;
- 2.2×10^{11} W in the Indian Ocean.

Thus, the sum for the entire World Ocean is 8.1×10^{11} W, which is approximately $\frac{1}{4}$ of the energy dissipation of the M_2 barotropic tide.

One of the first estimates of the total amount of the barotropic tide dissipation given by Cartwright [*Cartwright*, 1977] was 4.3×10^{12} W. Previously it was considered that tidal energy generally dissipates in the shallow seas. More recent astronomical estimates give a smaller value of tidal energy dissipation of the M_2 tide. The review papers by Munk and Wunsch [*Munk and Wunsch*, 1998] and Garrett [*Garrett*, 2003] emphasize the role of mid-oceanic ridges in the generation of internal tide. Egbert and Ray [*Egbert and Ray*, 2000, 2001] analyzed tidal elevation in the global ocean and estimated the total rate of the dissipation of tidal energy as 2.5 TW (1 TW = 10^{12} W) for the lunar semidiurnal tide M_2, 3.2 TW for all lunar tides. Much smaller energy (0.2 TW) dissipates in the atmosphere and solid Earth. Later estimates reported by Egbert and Ray [*Egbert and Ray*, 2003] indicate that the total dissipation of the M_2 tide is 2.435 TW, of which 1.649 TW dissipates in the shallow seas and 0.782 TW in the deep ocean. Kantha and Tierney [*Kantha and Tierney*, 1997] suggest on the basis of altimetric observations that the total energy of the M_2 baroclinic tide is 50 PJ, while the dissipation is 360 GW (3.6×10^{11} W).

Baines [*Baines*, 1982] estimated that less than 1% of semidiurnal tide energy (1.73×10^{10} W) is transferred to internal tides over continental slopes. Bell [*Bell*, 1975] estimated that about 10% of the tidal energy goes to internal tides over uneven abyssal topography in deep basins.

Let us consider the characteristic regions of very strong internal tides.

3. Regions of intense internal tides

3.1. Mascarene Ridge

The Mascarene Ridge is considered one of the regions, where internal tides of high energy are generated. The array of moorings was deployed in March 1987 assuming that the internal tide is generated by barotropic tidal currents in the underwater passage between the Saya de Malha and Nazareth banks [*Morozov and Vlasenko*, 1996]. The measurements confirmed the existence of large-amplitude internal tides. The mooring array of six moorings was extended in the direction to the southeast from the strait between the two banks. A scheme of location of moorings over bottom topography near the banks of the Mascarene Ridge is shown in Figure 2.

The vertical displacements caused by the internal tide were estimated from the temperature time series and vertical temperature gradient. Their mean amplitude at a depth of 1200 m was 0.2°C, which gives vertical displacements of the water particles equal to

120 m and correspondingly the amplitude of the displacement from the mean position as high as 60 m.

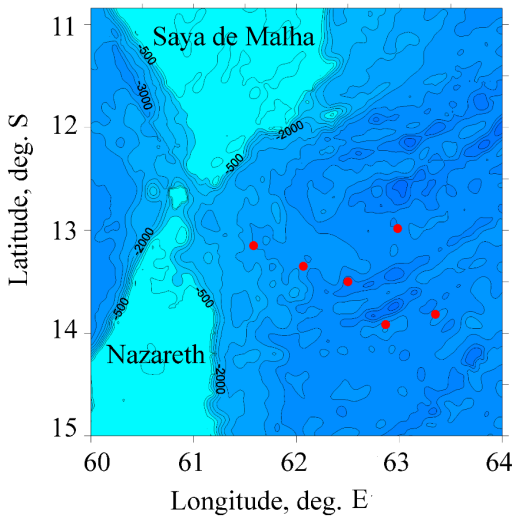

Figure 2. Bottom topography near the shallow banks of the Mascarene Ridge (m) and moorings east of the ridge. Depth contour lines are shown at depths of 500, 1000, 1500, 2000, 3000, 3500, and 4000 m. Locations of moorings are shown with red dots.

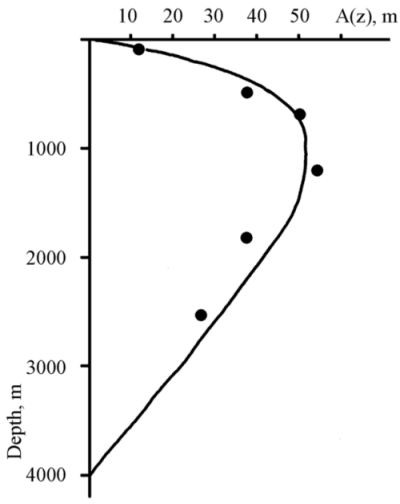

Figure 3. Amplitudes of semidiurnal internal waves near the Mascarene Ridge. The curve is the eigen function of the first mode (Equation 1). It was normalized by the maximum to fit the data of measured vertical displacements; the black dots show measured amplitudes of internal tide at the easternmost mooring.

Below we will analyze vertical distribution of semidiurnal internal tide amplitudes. A graph of the eigen function for the oscillations of the first mode is shown in Figure 3. It was calculated by the numerical integration of the equation for the vertical velocity (w) caused by internal waves at realistic stratification $N(z)$ and zero boundary conditions for vertical velocity at the surface and bottom [*LeBlond and Mysak*, 1978]:

$$\frac{d^2w}{dz^2} + \frac{N^2(z)}{g}\frac{dw}{dz} + \frac{N^2(z)-\omega^2}{\omega^2-f^2}wk^2 = 0, \quad (1)$$

where, $N^2(z)$ is the squared Brunt-Väisälä frequency based on the CTD data; ω is the semidiurnal frequency, f is the Coriolis parameter, and k is the horizontal wave number.

The theoretical wavelength of the first mode of internal tidal wave based on the integration of this equation was equal to 130 km, and the phase velocity was 2.9 m/s. The amplitudes of internal waves were also estimated from the spectra of time series at different depths on the easternmost mooring. Temperature fluctuations at semidiurnal frequency were divided by the vertical gradient of temperature; thus, vertical amplitudes of water particle displacements were estimated.

The wavelength and direction of propagation of internal tides were estimated based on the spatiotemporal spectra at the semidiurnal tidal frequency. They were calculated on the basis of measurements at six moorings (serving as an antenna for internal tides) at several levels using the method suggested by [*Barber*, 1963]. The wavelength of internal tide was 140–150 km, and its direction from the strait between the banks was 110°. Why are the amplitudes of internal tide so large over the Mascarene Ridge? Because the barotropic tide is strong, tidal currents are almost normal to the ridge, the tops of the ridges are shallow, while the surrounding waters are deep, and the stratification is strong.

3.2. Aleutian Ridge

Cummins et al. [*Cummins et al.*, 2001] used satellite altimetry to analyze internal tides radiated from the Aleutian Ridge. The authors reported coherent propagation of semidiurnal internal tides in the southern direction over a distance of at least 1100 km. The strongest energy fluxes occur in the vicinity of the Amutka Pass (52° N, 172° W).

The moorings were deployed during the GARS, FOCI, and NPBC experiments over the continental slopes of Alaska and the Aleutian Islands. The amplitude of internal tides at a depth of 1000 m was estimated at 70 m, while at a distance of 100 km from the slope the amplitude was 50 m. Locations of moorings are shown in Figure 4 [*Morozov*, 2018].

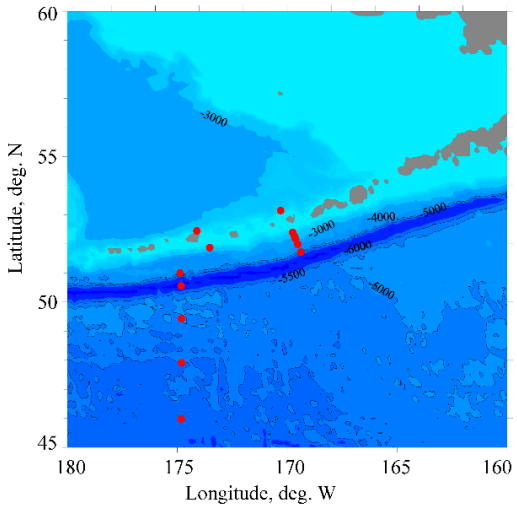

Figure 4. Bottom topography in the study site near the Aleutian Ridge and locations of moorings. Depth contour lines are shown at depths of 3000, 4000, 5000, 5500, and 6000 m. Land and islands are shown with gray color. Locations of moorings are shown with red dots.

A strong tidal flow propagates through the passes between the islands generating intense internal tides when overflowing the bottom slopes. A mooring at 52°24' N, 169°45' W deployed on the southern slope of the Aleutian Islands over a depth of 1050 m recorded the amplitudes of internal tides exceeding 150 m at a depth of 560 m. The records from another mooring over a depth of 2000 m showed amplitudes in the range 150–200 m. At a depth of 3000 m, the amplitudes decreased half of the initial amplitude (70–80 m) and after further spreading to a depth of 6000 m, they decreased to 25 m.

3.3. South China Sea

Several experiments were carried out in the South China Sea to study internal waves. The Luzon Strait is known as a strong generation region of internal tides due to the existence of two steep submarine ridges along the north-south direction. Internal tides generated over the pair of ridges propagate in both directions to the South China and Philippine seas. Many field studies with moored thermistor strings and ADCPs, satellite and radar observations, and model simulations were dedicated to this region of strong internal tides together with the theoretical research [*Fang et al.*, 2015; *Huan Lee et al.*, 2012; *Kerry et al.*, 2016; *Mercier et al.*, 2013; *Niwa and Hibiya*, 2004; *Orr and Mignerey*, 2003; *Ramp et al.*, 2004]. Internal tides generated over the slopes of these two submarine ridges propagate both sides. Internal tides propagating to the west of the Luzon Strait are very strong. Those internal tides propagating to the east are less intense. Analysis performed by Jan et al. [*Jan et al.*, 2008] revealed that strong internal tides are generated over the slopes of the eastern (70%) and western (30%) ridges. The results of experiments reported by Ramp et al. [*Ramp et al.*, 2004] report that the amplitudes of internal tides reached 50 m. Alford with coauthors [*Alford et al.*, 2015] report about the observations of internal tides at 20°30′ N, 119°00 E. The measurements reveal the existence of greater than 200-m high breaking internal waves in the region of generation. Many other publications report about amplitudes exceeding 100 m.

3.4. Gibraltar Strait

The flow in the Strait of Gibraltar (Figure 5) is characterized by a two-layer system of opposite currents that exists due to the difference in sea level and water density between the Atlantic Ocean and the Mediterranean Sea. Due to high water temperature evaporation of water in the Mediterranean is intense. Approximately 50 cm of water column evaporates during one year. This loss is compensated by the surface currents from the Atlantic Ocean. The velocities of this flow reach 40 cm/s. The flow changes its direction to the opposite at a depth of 100 m. A deep-water current of more saline Mediterranean Water flows into the ocean owing to the difference in water density. The velocities of this current in the lower layer reach 85 cm/s. The velocity maximum is close to the bottom. A barotropic tidal wave with mean velocities in the range 70-80 cm/s propagates through the strait. Strong internal tides are generated when the currents of the barotropic tide overflow transverse Camarinal Sill in the middle of the Strait of Gibraltar [*Bryden et al.*, 1994; *Farmer and Armi*, 1988; *Morozov et al.*, 2002].

The measurements over the Camarinal Sill reported by Boyce [*Boyce*, 1975] and Bockel [*Bockel*, 1962] indicate that the amplitudes of internal tides over the slopes of the sill are as high as 200 m.

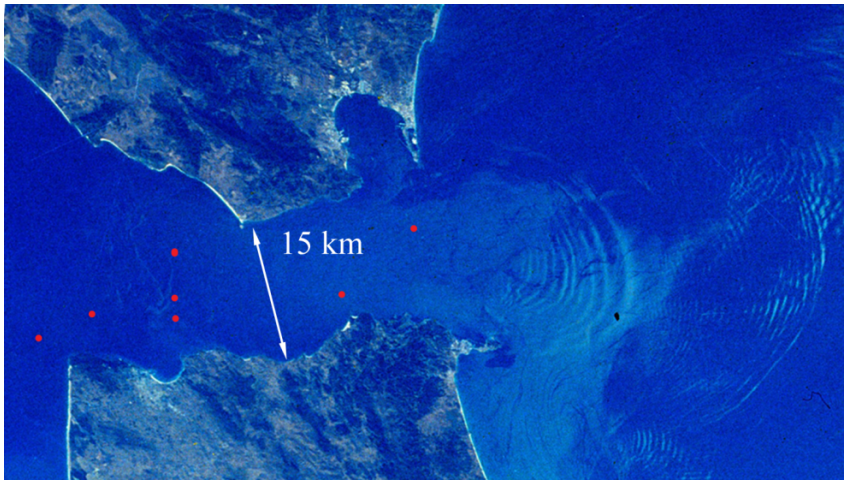

Figure 5. Satellite photo of the Strait of Gibraltar and surface manifestations of internal waves best seen in the eastern part. Red dots indicate locations of moorings in 1985–1986.

Analysis of moored temperature measurements shows that the displacement of the 13°C isotherm gives the best illustration pattern because this isotherm always remains within the depth interval of measurements. The vertical excursion of water particles (isotherm 13°C) ranges from 100 to 300 m depth. Superposition of the diurnal and semidiurnal tidal components based on the data from July 2 to July 31, 1986, is clearly seen in Figure 6.

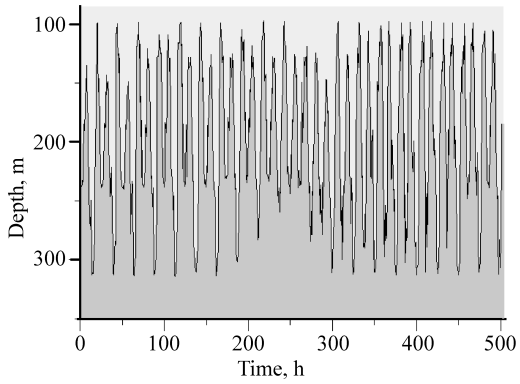

Figure 6. Depth variation of the 13°C isotherm over the Camarinal Sill from July 2 to July 31, 1986. Adopted from [*Morozov et al.*, 2002].

The internal tidal oscillations are observed over the sill exactly at the source of their generation; hence we conclude that these waves are forced internal oscillations, which transform into free propagating waves east and west of the sill. Internal tide waves lose their energy while propagating to the east and west from the Camarinal Sill. After propagating 50 km from the sill to the west, the amplitude of internal tides decreases three times.

However, strong internal tides here do not make any notable contribution to the internal wave energy balance in the ocean. The Strait of Gibraltar from the point of view of the global processes can be interpreted as a point source unlike quasi-linear sources of submarine ridges.

4. Decay of internal tides and global map of internal tide amplitudes

We have considered the estimates of energy fluxes of internal tides from most of the submarine ridges and estimated the amplitudes and energies of internal tides. The highest energies were revealed at those submarine ridges where the currents of the barotropic tide are normal to the ridge, and the geometry of the ridge intensifies generation of internal tides if the slopes of bathymetry are close to the characteristic curves of internal tide. This usually occurs near the crests if they are relatively close to the surface while the surrounding waters are deep. The energy of internal tides radiated from the submarine ridges is estimated as quarter of the barotropic tide dissipation. While propagating from the ridges internal tides lose their energy and their amplitude decreases. One of the goals of this study was to construct a global map of amplitudes of semidiurnal internal tides. In addition to the estimates of energy fluxes from submarine ridges as the sources areas we need estimates of energy decay in the course of propagation of internal tides. These estimates were evaluated from those moored measurements where long arrays of moorings were deployed in the normal direction to the ridge.

Spatial decay of the energy of semidiurnal internal tides in different regions was performed using the method described in [*Lozovatsky et al.*, 2003]. The density of the kinetic energy of the horizontal components of internal tide was determined as the sum of squared amplitudes of velocity. The total energy density of internal tide was calculated using the following formula [*Holloway and Merrifield*, 2003; *Torgrimson and Hickey*, 1979]:

$$E_{TW}(z) = 0.25\rho\left(\overline{u_{IT}^2(z)} + \overline{v_{IT}^2(z)} + N^2(z)\overline{\zeta_{IT}^2(z)}\right). \quad (2)$$

Here, u_{IT}, v_{IT} are the amplitudes of the semidiurnal internal tide velocity components, ζ_{IT} are vertical displacements. Internal tide velocity components were calculated from the mooring data subtracting the barotropic tide velocities.

Horizontal velocities of the barotropic tide in the region were calculated using the OTIS tidal inversion software based on satellite data assimilation [*Egbert and Erofeeva*, 2002]. The barotropic tide velocities over the slopes of the ridge sometimes exceed 40 cm/s, while far away from the ridge they decrease to 1–2 cm/s.

We normalized the distances by the scale equal to the wavelength of the first mode λ = 145 km. Over a distance of 1000–1500 km the energy density of the internal tide in the main thermocline (1000–1200 m) decreases by a factor of 10 approximately from 1 J/m^3 to 0.1 J/m^3. This is approximately 15% loss of energy over one wavelength; hence, a 10-fold energy decrease occurs over a distance of 12 wavelengths.

We compared the energy decay of the internal tide in the Mascarene region with some other regions. The graphs of energy decay in the Kuroshio, Aleutian, Kermadec, and Mozambique regions, are shown in Figure 7. The energy level in each of the regions is different but the rate of energy decay is very similar to the one analyzed near the Mascarene Ridge. The graphs in Figure 7 show that the energy decay with distance is similar in different regions of the oceans.

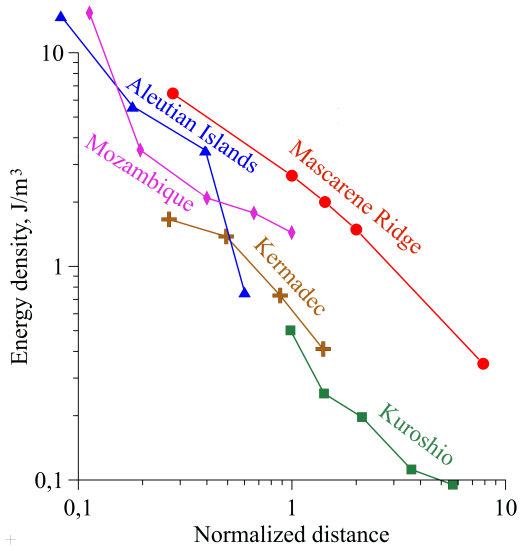

Figure 7. Combined graph of the semidiurnal internal tide energy decay with the distance from the source. The graph shows total energy density $E_{TW} + E_H + E_\zeta$ (see Equation 2) of the semidiurnal internal tide versus distance from the ridge. The distance from the ridge is normalized by the wavelength of the first mode λ = 145 km. The measurement depth is in the interval 1000–1200 m. Energy decay from the Mascarene Ridge is shown with circles of red color; from the Aleutian Islands with blue triangles; from the Mozambique slope with magenta diamonds; from the east Japan coast (Kuroshio) with green squares, and from the Kermadec Ridge (South Pacific) with brown crosses.

Decay of the semidiurnal internal tide amplitudes with distance in the regions of the Mascarene ridge and Aleutian Islands is shown in Figure 8. Decay is stronger near the source of internal tide generation. At greater distances from the ridge the amplitudes decrease slower, and eventually become close to 20 m, which is the background level of amplitudes worldwide.

The estimates of energy and amplitude decay made it possible to conclude that approximately 10% of internal tide energy and 5% of the amplitude are lost over a distance of one wavelength (~145 km). In deep basins far from the sources the energies of semidiurnal internal tide approach the natural background level [*Garrett and Munk*, 1972], 1972]. Thus, the waves propagate over 12–15 wavelengths. After evaluating the estimates of internal tide energy flux and decay of internal tides over distance it was possible to construct a map

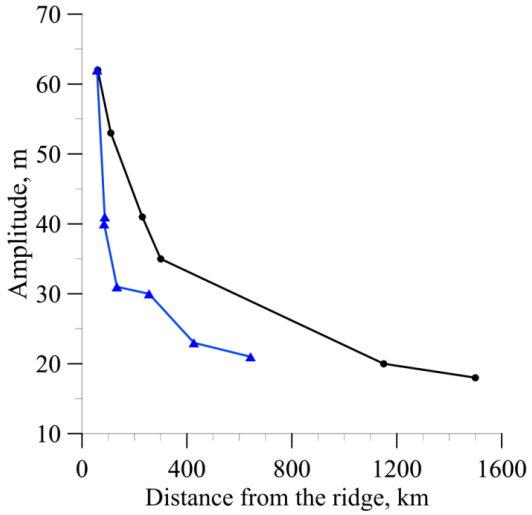

Figure 8. Combined graph of the semidiurnal internal tide amplitude decay with the distance from the Mascarene Ridge (black line and circles) and Aleutian Islands (blue line and triangles) based on the data of moorings.

of internal tide amplitudes in the ocean (Figure 9). The map is based on modeling and measurements. The largest amplitudes were found near submarine ridges. Several ridges in the ocean make the greatest contribution to the global energy balance of internal tide and dissipation of the barotropic tide. These ridges include the Mascarene Ridge, Aleutian Islands, Hawaii Islands, Kusu Palau Ridge, Mid-Atlantic Ridge in the South Atlantic, great Meteor Banks, and ridges in the Luzon Strait. The map is very general because it shows only the outline of the amplitude distribution. The amplitudes should be considered as "vertically averaged" and also "time averaged" over a half-month (spring-neap) time scale.

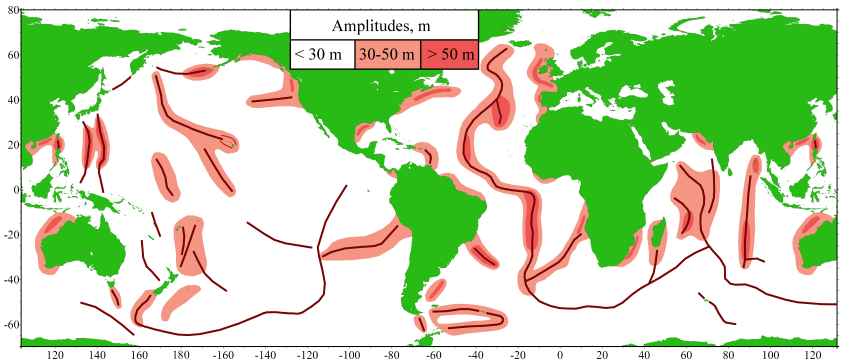

Figure 9. World map of the amplitudes of semidiurnal internal tides (meters). Submarine ridges are shown with heavy brown lines. The regions of the semidiurnal internal tide amplitudes exceeding 50 and 30 m (peak-to-peak) are shown in dark and light brown colors, respectively.

5. Conclusions

The major generation of internal tides occurs near submarine ridges. The highest energies were revealed at those submarine ridges where the currents of the barotropic tide are normal to the ridge, and the geometry of the ridge intensifies generation of internal tides if the slopes of bathymetry are close to the characteristic curves of internal tide. This usually occurs near the crests if they are relatively close to the surface while the surrounding waters are deep. The energy of internal tides radiated from the submarine ridges is estimated as quarter of the barotropic tide dissipation. The balance of tide dissipation energy has been closed. A quarter of the tide dissipation energy is transferred to internal tides. Previously it was considered that the major part of the barotropic tide dissipates in shallow seas, but

the balance was not closed. A map of the amplitudes of tidal internal waves in the ocean has been constructed.

Acknowledgments. The study was carried out within the framework of State Assignment FMWE-2024-0016 (ship measurements) and supported by the Russian Science Foundation grant no. 21-77-20004 (field data analysis and interpretation).

References

Alford, M. H., T. Peacock, J. A. MacKinnon, J. D. Nash, M. C. Buijsman, L. R. Centurioni, S.-Y. Chao, M.-H. Chang, D. M. Farmer, O. B. Fringer, K.-H. Fu, P. C. Gallacher, H. C. Graber, K. R. Helfrich, S. M. Jachec, C. R. Jackson, J. M. Klymak, D. S. Ko, S. Jan, T. M. S. Johnston, S. Legg, I.-H. Lee, R.-C. Lien, M. J. Mercier, J. N. Moum, R. Musgrave, J.-H. Park, A. I. Pickering, R. Pinkel, L. Rainville, S. R. Ramp, D. L. Rudnick, S. Sarkar, A. Scotti, H. L. Simmons, L. C. St. Laurent, S. K. Venayagamoorthy, Y.-H. Wang, J. Wang, Y. J. Yang, T. Paluszkiewicz, and T.-Y. (David) Tang (2015), The formation and fate of internal waves in the South China Sea, *Nature*, *521*(7550), 65–69, https://doi.org/10.1038/nature14399.

Baines, P. G. (1982), On internal tide generation models, *Deep Sea Research Part A. Oceanographic Research Papers*, *29*(3), 307–338, https://doi.org/10.1016/0198-0149(82)90098-X.

Barber, N. F. (1963), The directional resolving power of an array of wave detectors, in *Ocean Wave Spectra*, pp. 137–150, Prentice Hall, NY, Engelwood Cliffs.

Bell, T. H. (1975), Topographically generated internal waves in the open ocean, *Journal of Geophysical Research*, *80*(3), 320–327, https://doi.org/10.1029/JC080i003p00320.

Bockel, M. (1962), Travaux oceanographiques de l'"Origny" a Gibralter, in *Campagne Intemationale 15 Mai - 15 Juin 1961. I. Partie: Hydrologic dans le deroit*, pp. 325–329, Cahiers Oceanographie.

Boyce, F. M. (1975), Internal waves in the Straits of Gibraltar, *Deep Sea Research and Oceanographic Abstracts*, *22*(9), 597–610, https://doi.org/10.1016/0011-7471(75)90047-9.

Briscoe, M. G. (1975), Preliminary results from the trimoored internal wave experiment (IWEX), *Journal of Geophysical Research*, *80*(27), 3872–3884, https://doi.org/10.1029/JC080i027p03872.

Bryden, H. L., J. Candela, and T. H. Kinder (1994), Exchange through the Strait of Gibraltar, *Progress in Oceanography*, *33*(3), 201–248, https://doi.org/10.1016/0079-6611(94)90028-0.

Cairns, J. L., and E. C. LaFond (1966), Periodic motions of the seasonal thermocline along the southern California coast, *Journal of Geophysical Research*, *71*(16), 3903–3915, https://doi.org/10.1029/JZ071i016p03903.

Cartwright, D. E. (1977), Oceanic tides, *Reports on Progress in Physics*, *40*(6), 665–708, https://doi.org/10.1088/0034-4885/40/6/002.

Cummins, P. F., J. Y. Cherniawsky, and M. G. G. Foreman (2001), North Pacific internal tides from the Aleutian Ridge: Altimeter observations and modeling, *Journal of Marine Research*, *59*(2), 167–191, https://doi.org/10.1357/002224001762882628.

Egbert, G. D., and S. Y. Erofeeva (2002), Efficient Inverse Modeling of Barotropic Ocean Tides, *Journal of Atmospheric and Oceanic Technology*, *19*(2), 183–204, https://doi.org/10.1175/1520-0426(2002)019<0183:EIMOBO>2.0.CO;2.

Egbert, G. D., and R. D. Ray (2000), Significant dissipation of tidal energy in the deep ocean inferred from satellite altimeter data, *Nature*, *405*(6788), 775–778, https://doi.org/10.1038/35015531.

Egbert, G. D., and R. D. Ray (2001), Estimates of M2 tidal energy dissipation from TOPEX/Poseidon altimeter data, *Journal of Geophysical Research: Oceans*, *106*(C10), 22,475–22,502, https://doi.org/10.1029/2000JC000699.

Egbert, G. D., and R. D. Ray (2003), Semi-diurnal and diurnal tidal dissipation from TOPEX/Poseidon altimetry, *Geophysical Research Letters*, *30*(17), https://doi.org/10.1029/2003GL017676.

Fang, Y., Y. Hou, and Z. Jing (2015), Seasonal characteristics of internal tides and their responses to background currents in the Luzon Strait, *Acta Oceanologica Sinica*, *34*(11), 46–54, https://doi.org/10.1007/s13131-015-0747-z.

Farmer, D. M., and L. Armi (1988), The flow of Atlantic water through the Strait of Gibraltar, *Progress in Oceanography*, *21*(1), 1–103, https://doi.org/10.1016/0079-6611(88)90055-9.

Garrett, C. (2003), Internal Tides and Ocean Mixing, *Science*, *301*(5641), 1858–1859, https://doi.org/10.1126/science.1090002.

Garrett, C., and E. Kunze (2007), Internal Tide Generation in the Deep Ocean, *Annual Review of Fluid Mechanics*, *39*(1), 57–87, https://doi.org/10.1146/annurev.fluid.39.050905.110227.

Garrett, C., and W. Munk (1972), Space-Time scales of internal waves, *Geophysical Fluid Dynamics*, *3*(3), 225–264, https://doi.org/10.1080/03091927208236082.

Hibiya, T. (2004), Internal Wave Generation by Tidal Flow over a Continental Shelf Slope, *Journal of Oceanography*, *60*(3), 637–643, https://doi.org/10.1023/B:JOCE.0000038356.45342.6c.

Holloway, P. E., and M. A. Merrifield (2003), On the spring-neap variability and age of the internal tide at the Hawaiian Ridge, *Journal of Geophysical Research: Oceans*, *108*(C4), https://doi.org/10.1029/2002JC001486.

Huan Lee, I., Y. Wang, Y. Yang, and D. Wang (2012), Temporal variability of internal tides in the northeast South China Sea, *Journal of Geophysical Research: Oceans*, *117*(C2), https://doi.org/10.1029/2011JC007518.

Jan, S., R.-C. Lien, and C.-H. Ting (2008), Numerical study of baroclinic tides in Luzon Strait, *Journal of Oceanography*, *64*(5), 789–802, https://doi.org/10.1007/s10872-008-0066-5.

Johnston, T. M. S., M. A. Merrifield, and P. E. Holloway (2003), Internal tide scattering at the Line Islands Ridge, *Journal of Geophysical Research: Oceans*, *108*(C11), https://doi.org/10.1029/2003JC001844.

Kantha, L. H., and C. C. Tierney (1997), Global baroclinic tides, *Progress in Oceanography*, *40*(1–4), 163–178, https://doi.org/10.1016/S0079-6611(97)00028-1.

Kerry, C. G., B. S. Powell, and G. S. Carter (2016), Quantifying the Incoherent M2 Internal Tide in the Philippine Sea, *Journal of Physical Oceanography*, *46*(8), 2483–2491, https://doi.org/10.1175/JPO-D-16-0023.1.

Krauss, W. (1966), *Interne Wellen*, Gebrüder Borntraeger.

LaFond, E. C. (1961), The isotherm follower, *Journal of Marine Research*, *19*(1), 33–39.

LeBlond, P. H., and L. A. Mysak (Eds.) (1978), *Waves in the Ocean*, Elsevier.

Lee, W. H. K., and C. S. Cox (1966), Time variation of ocean temperatures and its relation to internal waves and oceanic heat flow measurements, *Journal of Geophysical Research*, *71*(8), 2101–2111, https://doi.org/10.1029/JZ071i008p02101.

Lozovatsky, I. D., E. G. Morozov, and H. J. S. Fernando (2003), Spatial decay of energy density of tidal internal waves, *Journal of Geophysical Research: Oceans*, *108*(C6), https://doi.org/10.1029/2001JC001169.

Mercier, M. J., L. Gostiaux, K. Helfrich, J. Sommeria, S. Viboud, H. Didelle, S. J. Ghaemsaidi, T. Dauxois, and T. Peacock (2013), Large-scale, realistic laboratory modeling of M2 internal tide generation at the Luzon Strait, *Geophysical Research Letters*, *40*(21), 5704–5709, https://doi.org/10.1002/2013GL058064.

Morozov, E. G. (1988), Generation of internal tides over submarine ridges, *Oceanological Researches*, *41*, 55–67 (in Russian).

Morozov, E. G. (1990), Geographical variability of internal waves, *Oceanological Researches*, *43*, 48–68 (in Russian).

Morozov, E. G. (1995), Semidiurnal internal wave global field, *Deep Sea Research*, *42*(1), 135–148.

Morozov, E. G. (2006), Internal Tides. Global field of internal tides and mixing caused by internal tides, in *Waves in Geophysical Fluids*, pp. 271–332, Springer, Wein, New York.

Morozov, E. G. (2018), *Oceanic Internal Tides: Observations, Analysis and Modeling*, Springer International Publishing, https://doi.org/10.1007/978-3-319-73159-9.

Morozov, E. G., and V. I. Vlasenko (1996), Extreme tidal internal waves near the Mascarene ridge, *Journal of Marine Systems*, *9*(3–4), 203–210, https://doi.org/10.1016/S0924-7963(95)00042-9.

Morozov, E. G., K. Trulsen, M. G. Velarde, and V. I. Vlasenko (2002), Internal Tides in the Strait of Gibraltar, *Journal of Physical Oceanography*, *32*(11), 3193–3206, https://doi.org/10.1175/1520-0485(2002)032<3193:ITITSO>2.0.CO;2.

Munk, W. H. (1966), Abyssal recipes, *Deep Sea Research and Oceanographic Abstracts*, *13*(4), 707–730, https://doi.org/10.1016/0011-7471(66)90602-4.

Munk, W. H., and C. Wunsch (1998), Abyssal recipes II: energetics of tidal and wind mixing, *Deep Sea Research Part I: Oceanographic Research Papers*, *45*(12), 1977–2010, https://doi.org/10.1016/S0967-0637(98)00070-3.

Nansen, F. (1902), *The Oceanography of the North Polar BasinNorwegian North Polar Expedition 1893 - 1896 : scientific results*, vol. 9, Longmans and Green.

Niwa, Y., and T. Hibiya (2004), Three-dimensional numerical simulation of M2 internal tides in the East China Sea, *Journal of Geophysical Research: Oceans*, *109*(C4), https://doi.org/10.1029/2003JC001923.

Orr, M. H., and P. C. Mignerey (2003), Nonlinear internal waves in the South China Sea: Observation of the conversion of depression internal waves to elevation internal waves, *Journal of Geophysical Research: Oceans*, *108*(C3), https://doi.org/10.1029/2001JC001163.

Phillips, O. M. (1977), *The Dynamics of the Upper Ocean*, ii ed., Syndics of the Cambridge University Press, England.

Ramp, S. R., T. Y. Tang, T. F. Duda, J. F. Lynch, A. K. Liu, C.-S. Chiu, F. L. Bahr, H.-R. Kim, and Y.-J. Yang (2004), Internal Solitons in the Northeastern South China Sea Part I: Sources and Deep Water Propagation, *IEEE Journal of Oceanic Engineering*, *29*(4), 1157–1181, https://doi.org/10.1109/JOE.2004.840839.

Sjöberg, B., and A. Stigebrandt (1992), Computations of the geographical distribution of the energy flux to mixing processes via internal tides and the associated vertical circulation in the ocean, *Deep Sea Research Part A. Oceanographic Research Papers*, *39*(2), 269–291, https://doi.org/10.1016/0198-0149(92)90109-7.

Summers, H. J., and K. O. Emery (1963), Internal waves of tidal period off Southern California, *Journal of Geophysical Research*, *68*(3), 827–839, https://doi.org/10.1029/JZ068i003p00827.

Tareev, B. A. (1966), Dynamics of internal gravity waves in a continuously stratified ocean, *Izvestiya, Academy of Sciences, USSR. Atmospheric and Oceanic Physics*, *2*(10), 1064–1075.

Torgrimson, G. M., and B. M. Hickey (1979), Barotropic and Baroclinic Tides over the Continental Slope and Shelf off Oregon, *Journal of Physical Oceanography*, *9*(5), 945–961, https://doi.org/10.1175/1520-0485(1979)009<0945:BABTOT>2.0.CO;2.

Wunsch, C. (1975a), Deep ocean internal waves: What do we really know?, *Journal of Geophysical Research*, *80*(3), 339–343, https://doi.org/10.1029/JC080i003p00339.

Wunsch, C. (1975b), Internal tides in the ocean, *Reviews of Geophysics*, *13*(1), 167–182, https://doi.org/10.1029/RG013i001p00167.